Mechanism of intermetallic charge transfer and bond disproportionation in BiNiO$_3$ and PbNiO$_3$ revealed by hard x-ray photoemission spectroscopy

Tatsuya Yamaguchi [1] Mizuki Furo,[1] Yuki Sakai,[2,3] Takumi Nishikubo,[2,3] Hajime Hojo,[4] Masaki Azuma,[2,3]
Kengo Oka [5,6] Daisuke Mori,[7,8] Yoshiyuki Inaguma [7] Masaichiro Mizumaki,[9]
Kento Yamamoto,[10] Jan Kuneš [11,12] Takashi Mizokawa,[10] and Atsushi Hariki [1]

[1]*Department of Physics and Electronics, Graduate School of Engineering, Osaka Metropolitan University*
1-1 Gakuen-cho, Nakaku, Sakai, Osaka 599-8531, Japan
[2]*Kanagawa Institute of Industrial Science and Technology (KISTEC), Ebina 243-0435, Japan*
[3]*Materials and Structures Laboratory, Institute of Innovative Research,*
Tokyo Institute of Technology 4259 Nagatsuta, Midori, Yokohama 226-8501, Japan
[4]*Department of Advanced Materials Science and Engineering, Faculty of Engineering Sciences, Kyushu University,*
6-1 Kasuga-koen, Kasuga, Fukuoka 816-8580, Japan
[5]*Department of Applied Chemistry, Faculty of Science and Engineering, Chuo University,*
1-13-27 Kasuga, Bunkyo-ku, Tokyo 112-8551, Japan
[6]*Department of Applied Chemistry, Faculty of Science and Engineering, Kindai University,*
3-4-1 Kowakae, Higashi-Osaka, Osaka 577-8502, Japan
[7]*Department of Chemistry, Faculty of Science, Gakushuin University, 1-5-1 Mejiro, Toshima-ku, Tokyo 171-8588, Japan*
[8]*Department of Applied Chemistry, Graduate School of Engineering, Mie University, Tsu, Mie 514-8507, Japan*
[9]*Institute of Industrial Nanomaterials, Kumamoto University 2-39-1 Kurokami Chuo-ku Kumamoto 860-8555, Japan*
[10]*Department of Applied Physics, Waseda University, 3-4-1 Okubo, Shinjuku-ku, Tokyo 169-8555, Japan*
[11]*Institute of Solid State Physics, TU Wien, 1040 Vienna, Austria*
[12]*Department of Condensed Matter Physics, Faculty of Science, Masaryk University, Kotlářská 2, 611 37 Brno, Czechia*

Perovskites with Bi or Pb on the A site host a number of interesting and yet to be understood phenomena such as negative thermal expansion in BiNiO$_3$. We employ hard x-ray photoemission spectroscopy of Ni 2p core level as well as valence band to probe the electronic structure of BiNiO$_3$ and PbNiO$_3$. The experimental results supported by theoretical calculations using dynamical mean-field theory reveal essentially identical electronic structure of the Ni–O subsystem typical of Ni^{2+} charge-transfer insulators. The two materials are distinguished by filling of the Bi(Pb)–O antibonding states in the vicinity of the Fermi level, which is responsible for the Bi disproportionation in BiNiO$_3$ at ambient pressure and absence of similar behavior in PbNiO$_3$. The present experiments provide evidence for this conclusion by revealing the presence/absence of Bi/Pb 6s states at the top of the valence band in the two materials.

I. INTRODUCTION

The A sites of typical AMO$_3$ perovskite transition-metal oxides (TMOs) are occupied by divalent alkaline earth metal or trivalent Y or rare-earth ions, which act as electron donors and form ionic bonds with oxygen. Perovskites with Pb or Bi on the A site are different. The Pb or Bi ions play a more active role thanks to their ability to form covalent bonds with oxygen. Both Pb and Bi belong to so-called valence skippers, ions that prefer to adopt the 6s^0 (Pb^{4+}, Bi^{5+}) and 6s^2 (Pb^{2+}, Bi^{3+}) valence configurations while avoiding the 6s^1 (Pb^{3+}, Bi^{4+}) configuration. This behavior can be modelled with an attractive onsite interaction, negative U, within the 6s shell [1]. The origin of the negative U has been attributed to covalent bonding plus electron-lattice coupling [2] or nonlinear nonlocal screening [3].

Electronic structure calculations [4,5] have shown that valence skipping in perovskite TMOs is caused by Pb(Bi)–O hybridization, which leads to formation of a relatively narrow antibonding band. Its energy, determined by bonding-antibonding splitting, is sensitive to small changes of the Pb(Bi)–O bond lengths and therefore strongly coupled to the lattice [6]. Formal 6s^0 and 6s^2 valence configurations correspond to a situation where the antibonding band is located above and below the Fermi level E_F, respectively. The 6s^1 or partially filled configurations would amount to pinning of the antibonding band at E_F. Such states/structures are often unstable towards small changes of the Pb(Bi)–O lengths, which cause the antibonding states to move away from E_F. This is accompanied by transfer of electrons/holes to other orbitals, e.g., TM 3d ones. Alternatively, Pb(Bi)–O bond-length disproportionation splits the antibonding band away from E_F and leads to redistribution of charge among inequivalent Pb(Bi) ions. While the negative U picture also leads to valence skipping it does not account for the geometrical constraints and correlations between Pb(Bi)–O bond lengths due to the A sites sharing their oxygen neighbors and vice versa. This affects possible ordering patterns of 6s^2 and 6s^0 sites on the lattice [4,5] as well as dynamics of the 6s electrons.

The Pb(Bi)–O hybridization picture can be probed by studying the Pb(Bi) 6s spectra. To this end, we have measured the valence and core-level x-ray photoemission spectroscopy (XPS) spectra of closely related PbNiO$_3$ and BiNiO$_3$ and analyzed them with the help of electronic-structure calculations using local-density approximation (LDA) combined with dynamical mean-field theory (DMFT) method. We employ hard x-ray photoemission spectroscopy (HAXPES) which has large photoionization cross sections (CSs) for the Pb(Bi) 6s orbitals.

At ambient pressure BiNiO$_3$ is a good insulator [7] while PbNiO$_3$ shows a semiconducting behavior [8]. BiNiO$_3$ undergoes a pressure-driven metal-insulator transition (MIT) at the critical pressure 3.5 GPa [9,10], which has been identified as a new type of MIT driven by electron transfer from Bi to Ni and interpreted using the negative U picture [11,12]. At ambient pressure, BiNiO$_3$ is an insulator with two distinct Bi sites and formal valence Bi$_{0.5}^{3+}$Bi$_{0.5}^{5+}$Ni^{2+}O$_3$ [13]. At high pressure, it is a metal with formal valence Bi^{3+}Ni^{3+}O$_3$ [9,10]. PbNiO$_3$ takes formal valence Pb^{4+}Ni^{2+}O$_3$.

II. METHODS

A. Experimental method

Polycrystalline samples of BiNiO$_3$ and PbNiO$_3$ were prepared under high pressure [8]. HAXPES measurements for valence band and Ni 2p core level were performed at 300 K with photon energy of 7939.8 eV at the undulator beamlines BL47XU of SPring-8. For these measurements, hemispherical photoelectron analyzers (SES2002/R-4000) were used. The polycrystalline samples were fractured *in situ* for the XPS measurements. The binding energies were calibrated using Au 4$f_{7/2}$ peak (84.0 eV) and Fermi edge of gold reference samples. The total energy resolution was 280 meV.

B. Computational method

The valence-band and core-level XPS spectra are simulated using the LDA + DMFT method [14–16]. The computation starts with a standard LDA calculation using Wien2k [17] for the experimental crystal structures of PbNiO$_3$ ($Pbn2_1$ space group) [18] and BiNiO$_3$ ($P\bar{1}$ space group) [13]. In BiNiO$_3$, two inequivalent Bi sites [13] are present as shown in Fig. 1. The two Bi sites, with the shortest Bi–O bonds of 2.21 Å and 2.03 Å, are referred to as the "lone" and "pair" Bi ions hereafter.

Next, the LDA bands are mapped onto a tight-binding model spanning the Bi (Pb) 5d, 6s, 6p, Ni 3d, 4s, O 2s and 2p bands [19,20]. Although the low-energy electronic structures of the two compounds are governed by the Ni 3d, O 2p, and Bi (Pb) 6s states, the other orbitals can be observed in the HAXPES spectra due to hybridization. The tight-binding model is augmented with a local electron-electron interaction within the Ni 3d shell. We employ Hubbard U and Hund's J parameters of $(U, J) = (7.0$ eV, 1.1 eV) [21]. The double-counting correction μ_{dc} [16,22] is set to reproduce the experimental valence-band and core-level spectra as in Refs. [23–25]. The details can be found in the Supplementary Material (SM) [26]. The strong-coupling continuous-time quantum Monte Carlo impurity solver [27–29] of the Anderson impurity model
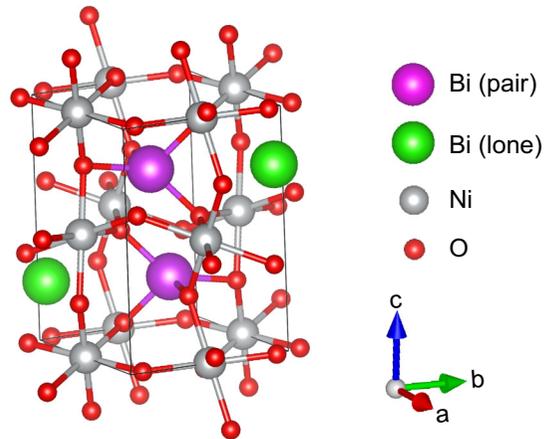

FIG. 1. Crystal structure of BiNiO$_3$ [13] visualized by VESTA [34].

(AIM) is used to compute Ni 3d self-energies $\Sigma(i\omega_n)$. The valence-band spectra and hybridization densities $\Delta(\omega)$ on the real-frequency axis are calculated from the local self-energy $\Sigma(\omega)$ analytically continued to the real-frequency axis using maximum entropy method [30,31].

The Ni 2p core-level XPS spectra are calculated using a configuration-interaction impurity solver [23,32,33] from the DMFT AIM augmented with the Ni 2p core orbitals and their interaction with the valence electrons. The hybridization densities $\Delta(\omega)$ are represented by 25 discrete levels (per spin and orbital).

III. RESULTS AND DISCUSSION

A. Core-level XPS

We start our discussion with Ni 2p core-level XPS spectra. Figure 2 shows the Ni 2p XPS spectra of BiNiO$_3$ and PbNiO$_3$ measured at room temperature. Overall spectral shapes are similar to those of typical Ni^{2+} oxides, such as NiO [35] and La$_2$NiO$_4$ [36]. Both the 2$p_{1/2}$ (884–868 eV) and 2$p_{3/2}$ (868–852 eV) contributions consist of a main line (ML) and a satellite (ST). The Ni 2$p_{3/2}$ ML in BiNiO$_3$ exhibits a shoulder on the higher-binding energy side, while the shoulder is less pronounced and the ML is more symmetric in PbNiO$_3$. Given that the Néel temperatures of 300 K in BiNiO$_3$ and 225 K in PbNiO$_3$ [8,13], we show the simulations for the antiferromagnetic insulating (AFI) phase for BiNiO$_3$ and the paramagnetic insulating (PMI) phase for PbNiO$_3$ in Fig. 2. Figure 3 shows that the spectra calculated within the same phase (i.e., AFI or PMI) are very similar in the two compounds, suggesting essentially identical electronic structures of Ni-O subsystems in BiNiO$_3$ and PbNiO$_3$.

We briefly discuss the physical origin of the observed core-level spectra. Sudden creation of a localized core hole triggers a dynamical charge response in the XPS final states, which amounts to charge transfer (CT) from surrounding ligands as well as distant Ni ions to the excited Ni site, conventionally referred to as CT screening. The two components in the ML originate from two CT screening processes: one from nearest-neighboring ligands and the other, at lower binding energy,
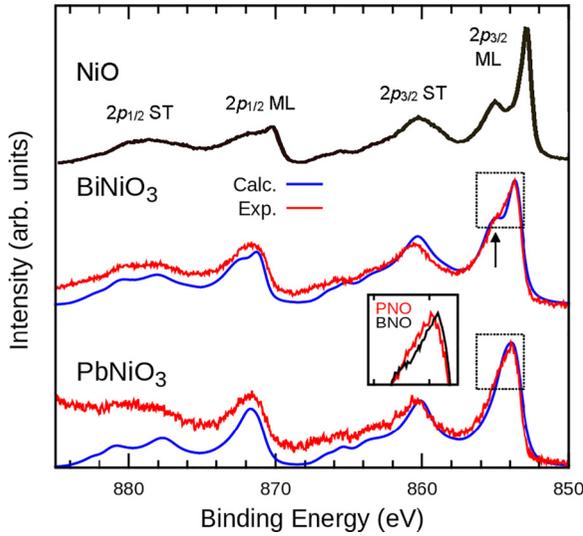
FIG. 2. The Ni $2p$ HAXPES experimental data (red) and the LDA + DMFT AIM calculations (blue) for $BiNiO_3$ in the AFI phase (middle) and $PbNiO_3$ (bottom) in the PMI phase. An arrow indicates the shoulder feature mentioned in the main text. The inset displays the magnified view of the Ni $2p_{3/2}$ ML in the experimental data for $PbNiO_3$ (PNO, red) and $BiNiO_3$ (BNO, black). The spectral broadening is considered using Gaussian of 300 meV and Lorentian of 300 meV (HWHM) in the calculated results. The Ni $2p$ XPS data of NiO [35] is shown for comparison (top). The Ni $2p_{3/2}$ ($2p_{1/2}$) main line (ML) and satellite (ST) are indicated.

from distant Ni ions, often called local and nonlocal screening, respectively [35,37,38]. The nonlocal CT screening in Ni^{2+} oxides [23,38] is less efficient in PMI than in AFI due to Pauli blocking, which explains the suppression of low-energy peak in PMI.

B. Valence-band XPS

Figure 4 shows the experimental and LDA + DMFT valence-band spectra of $BiNiO_3$ [40] and $PbNiO_3$. Soft x-ray XPS (SXPS) spectrum of $Bi_{0.95}La_{0.05}NiO_3$ measured
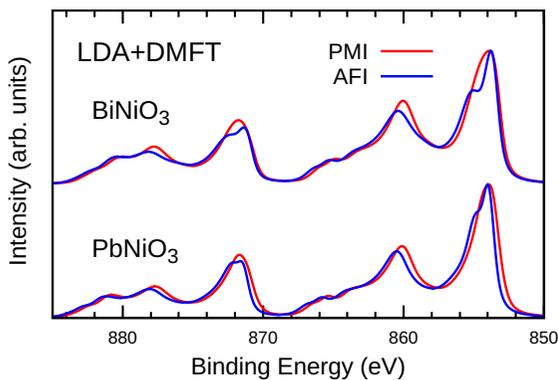

FIG. 3. The LDA + DMFT Ni $2p$ XPS spectra calculated for $BiNiO_3$ (top) and $PbNiO_3$ (bottom) in the paramagnetic insulating (red) and antiferromagnetic insulating (blue) phases.
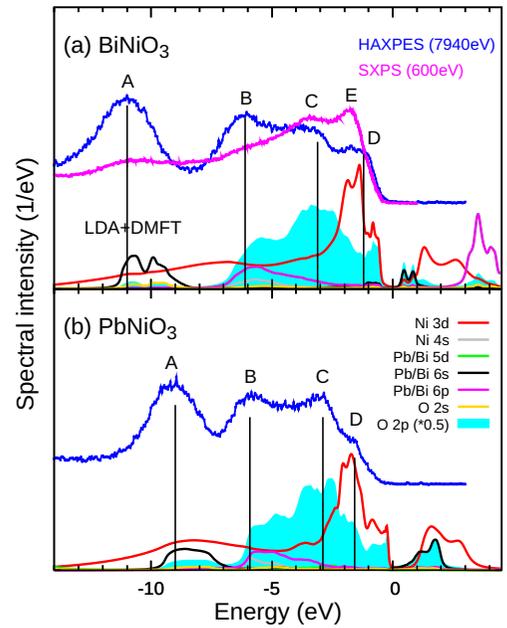

FIG. 4. The LDA + DMFT valence-band spectral intensities of (a) $BiNiO_3$ in the antiferromagnetic phase and (b) $PbNiO_3$ in the paramagnetic phase. The experimental valence-band spectra (blue) of $BiNiO_3$ [39,40] and $PbNiO_3$ are shown for comparison.

at photon energy of 600 eV [39] is shown for comparison. The difference between the spectra obtained with hard and soft x rays reflects the different photon-energy dependencies of the photoionization CSs for the constituent orbitals. The empirical CS values summarized in Table I show that while Ni $3d$ orbitals have large CS at 500 eV, at 7940 eV the Bi (Pb) CSs are dominant. This makes the hard x rays well suited to study the Bi and Pb $6s$ states.

We identify features labeled as A, B, C, D in the HAXPES spectra of $BiNiO_3$ and $PbNiO_3$. In addition, a feature E, enhanced in soft x-ray spectra, is attributed to the Ni $3d$ orbital

TABLE I. Subshell photoionization cross section σ at 8000 eV (hard x ray) and 500 eV (soft x ray) for relevant orbitals [42–44]. The differential cross section $d\sigma/d\Omega$ at 8000 eV is calculated taking the dipole parameter β for the angular distribution into account. To simulate the experimental geometry in the previous SXPS study in Ref. [39], β is not considered for $d\sigma/d\Omega$ at 500 eV.

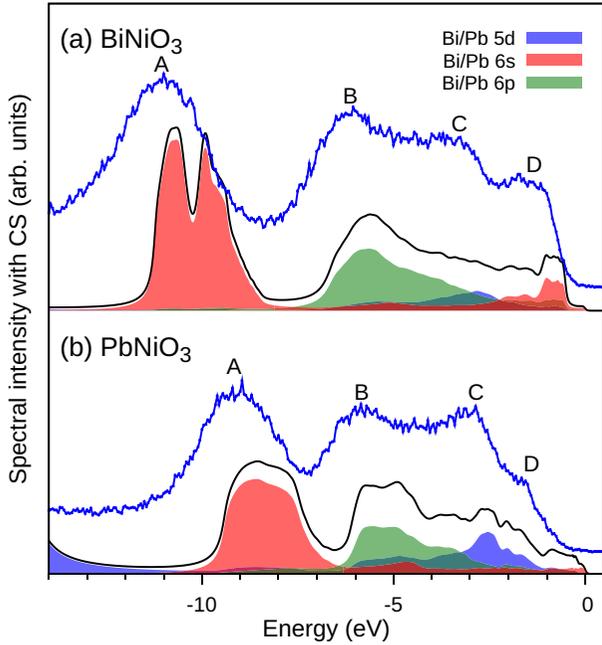|	8000 eV			500 eV	
	β	σ [b]	$d\sigma/d\Omega$ [b/sr]	σ [b]	$d\sigma/d\Omega$ [b/sr]
Ni $3d$	0.322	0.741	0.078	19.969	1.589
Ni $4s$	1.960	6.855	1.615	2.569	0.204
Bi $5d$	1.198	68.690	12.014	14.282	1.137
Bi $6s$	1.890	25.050	5.761	2.658	0.212
Bi $6p$	1.731	14.340	3.116	1.569	0.125
Pb $5d$	1.184	59.350	10.317	13.116	1.044
Pb $6s$	1.898	21.495	4.957	2.338	0.186
Pb $6p$	1.653	13.475	2.845	0.983	0.078
O $2s$	1.923	6.795	1.581	11.510	0.916
O $2p$	0.053	0.080	0.007	2.214	0.176

FIG. 5. The LDA + DMFT valence-band spectral intensities of (a) $BiNiO_3$ in the antiferromagnetic phase and (b) $PbNiO_3$ in the paramagnetic phase weighted with the CSs listed in Table I. The Fermi-Dirac function at 300 K is included in the theoretical spectra. The filled curves show the contributions of the Bi (Pb) $5d$, $6s$, and $6p$ states. The experimental HAXPES data (blue) of $BiNiO_3$ [40] and $PbNiO_3$ are shown for comparison.

FIG. 6. The valence-band spectra in (a) BiO_3 and (b) PbO_3 sublattice computed by removing the Ni $3d$ orbitals in the LDA + DMFT valence-band models in Figs. 4(a), (b). The Bi and Pb $6s$ spectral weights are magnified by the factor of 3. The solid (dashed) line in $BiNiO_3$ represents lone (pair) Bi site contribution.

contributions and matches well the position of the Ni $3d$ peak in the LDA + DMFT result. The peak *A* corresponds to Bi (Pb) $6s$ states—bonding state in the language of Bi(Pb)–O hybridization. On the other hand, peak *D* gains its weight in the HAXPES spectrum of $BiNiO_3$, peak *D* of $BiNiO_3$ can be assigned to Bi $6s$ or $6p$.

In order to identify the origin of features *B*, *C*, *D*, we weight the LDA + DMFT valence-band intensities with the CSs at 7940 eV in Fig. 5. An underestimate (~ 0.5 eV) of the binding energies of the feature *A* is due to uncertainty in the adopted approximation for the exchange-correlation potential [41]. Although the Bi (Pb) $5d$ and $6p$ states are positioned far below and above E_F, see SM [26], their CSs are extremely large in the hard x-ray regime, Table I. This together with a tiny hybridization with the valence band makes them apparent in the HAXPES spectra in the valence region. The simulated spectra in Fig. 5 show that the Bi or Pb $6p$ states are important for the feature *B*, while the $5d$ states give rise to the feature *C*. The shallower Pb $5d$ states could explain the enhanced intensity of the feature *C* in $PbNiO_3$ compared to that in $BiNiO_3$. The main qualitative difference between the HAXPES spectra of $BiNiO_3$ and $PbNiO_3$ is the enhanced spectral weight at the top of the valence band. The analysis of Fig. 5 links it to the presence of Bi $6s$ orbital character, while Pb $6s$ states are missing at the valence-band top in $PbNiO_3$. To isolate the physics of Bi(Pb) $6s$–O $2p$ bonding, we present, in Fig. 6, the Bi(Pb) $6s$ and O $2p$ spectral densities obtained with the Ni–O and Ni–Bi(Pb) hopping artificially switched off in the LDA + DMFT valence-band models in Fig. 4. Besides
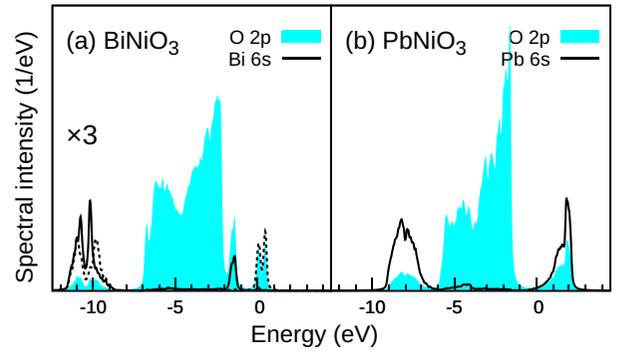
the quantitative differences consisting in shallower $6s$ states for lighter Pb and the resulting somewhat stronger covalent character of the Pb–O bond, there is a qualitative difference reflecting the disproportionation of the Bi sites. This leads to splitting of the antibonding band into states associated with the lone Bi site at lower and pair Bi sites at higher energies, consistent with the previous GGA + U and DMFT studies [4,45]. No splitting of the antibonding band takes place in $PbNiO_3$. This picture, necessarily with broader and richer structures in the $6s$ spectra, is preserved when Ni is fully included. The CT gap of Ni–O subsystem overlaps with lone-pair antibonding gap in $BiNiO_3$ and O $2p$-antibonding gap in $PbNiO_3$ in Fig. 4.

IV. CONCLUSIONS

We have presented a comparative study of two A-site active nickelates $BiNiO_3$ and $PbNiO_3$. The valence and Ni $2p$ core-level photoemission experiments supported by LDA + DMFT calculations reveal essentially identical electronic structures of Ni–O subsystems in the two compounds, characteristic of Ni^{2+} in charge-transfer systems such as NiO [46–48]. The main difference between the two compounds is derived from the Pb(Bi) $6s$ orbitals. The calculations find strong Pb(Bi)–O hybridization leading to bonding-antibonding splitting of almost 10 eV, with the antibonding states located within the charge-transfer gap. In $PbNiO_3$, electron counting places the Fermi level below the antibonding band, while in $BiNiO_3$ the Fermi level falls in the middle of the antibonding band. This situation in the latter is resolved by disproportionation of the Bi–O bonds, which gives rise to two distinct Bi sites, with antibonding states above and below the Fermi level.

Our main experimental result is the observation of the Bi–O antibonding states at the top of the valence band, which confirms the above mechanism of Bi disproportionation. We conclude our presentation by commenting on the relationship of the present description to the negative U model of valence skippers. The negative U model qualitatively explains presence (absence) of A-site disproportionation in $BiNiO_3$ ($PbNiO_3$). It can be viewed as an effective model for the Pb(Bi)–O antibonding states obtained by the process of integrating out the O states. However, in this process also nonlocal

interaction terms are expected to appear, e.g., due to O site having several Pb(Bi) neighbors. Such terms determine the pattern of disproportionated Bi ions on the lattice.

A question also arises about the negative U treatment of possible superconductivity in materials with valence skippers. Strong covalent bonds in systems with antibonding states at the Fermi level result in a strong electron-phonon coupling [6]. As in other such materials, superconductivity is competing with a structural instability. The capability of the negative U model to capture this competition appears questionable and we find that the full treatment of Pb(Bi)–O bonding without the effective $6s$ interaction U preferable.

[1] H. Matsuura, H. Mukuda, and K. Miyake, AAPPS Bulletin **32**, 30 (2022).

[2] P. W. Anderson, Phys. Rev. Lett. **34**, 953 (1975).

[3] C. M. Varma, Phys. Rev. Lett. **61**, 2713 (1988).

[4] A. Paul, A. Mukherjee, I. Dasgupta, A. Paramekanti, and T. Saha-Dasgupta, Phys. Rev. Lett. **122**, 016404 (2019).

[5] A. Hariki, K.-H. Ahn, and J. Kuneš, Phys. Rev. B **104**, 235101 (2021).

[6] J. M. An and W. E. Pickett, Phys. Rev. Lett. **86**, 4366 (2001).

[7] S. Ishiwata, M. Azuma, M. Hanawa, Y. Moritomo, Y. Ohishi, K. Kato, M. Takata, E. Nishibori, M. Sakata, I. Terasaki, and M. Takano, Phys. Rev. B **72**, 045104 (2005).

[8] Y. Inaguma, K. Tanaka, T. Tsuchiya, D. Mori, T. Katsumata, T. Ohba, K.-i. Hiraki, T. Takahashi, and H. Saitoh, J. Am. Chem. Soc. **133**, 16920 (2011).

[9] M. Azuma, W.-t. Chen, H. Seki, M. Czapski, S. Olga, K. Oka, M. Mizumaki, T. Watanuki, N. Ishimatsu, N. Kawamura, S. Ishiwata, M. G. Tucker, Y. Shimakawa, and J. P. Attfield, Nat. Commun. **2**, 347 (2011).

[10] M. Azuma, S. Carlsson, J. Rodgers, M. G. Tucker, M. Tsujimoto, S. Ishiwata, S. Isoda, Y. Shimakawa, M. Takano, and J. P. Attfield, J. Am. Chem. Soc. **129**, 14433 (2007).

[11] M. Naka, H. Seo, and Y. Motome, Phys. Rev. Lett. **116**, 056402 (2016).

[12] S. Kojima, J. Nasu, and A. Koga, Phys. Rev. B **94**, 045103 (2016).

[13] S. Ishiwata, M. Azuma, M. Takano, E. Nishibori, M. Takata, M. Sakata, and K. Kato, J. Mater. Chem. **12**, 3733 (2002).

[14] W. Metzner and D. Vollhardt, Phys. Rev. Lett. **62**, 324 (1989).

[15] A. Georges, G. Kotliar, W. Krauth, and M. J. Rozenberg, Rev. Mod. Phys. **68**, 13 (1996).

[16] G. Kotliar, S. Y. Savrasov, K. Haule, V. S. Oudovenko, O. Parcollet, and C. A. Marianetti, Rev. Mod. Phys. **78**, 865 (2006).

[17] P. Blaha, K. Schwarz, G. Madsen, D. Kvasnicka, and J. Luitz, *WIEN2k, An Augmented Plane Wave + Local Orbitals Program for Calculating Crystal Properties* (Karlheinz Schwarz, Techn. Universitat Wien, Austria, 2018).

[18] Y. Sakai, T. Nishikubo, T. Ogata, H. Ishizaki, T. Imai, M. Mizumaki, T. Mizokawa, A. Machida, T. Watanuki, K. Yokoyama, Y. Okimoto, S.-y. Koshihara, H. Das, and M. Azuma, Chem. Mater. **31**, 4748 (2019).

[19] J. Kuneš, R. Arita, P. Wissgott, A. Toschi, H. Ikeda, and K. Held, Comput. Phys. Commun. **181**, 1888 (2010).

[20] A. A. Mostofi, J. R. Yates, G. Pizzi, Y.-S. Lee, I. Souza, D. Vanderbilt, and N. Marzari, Comput. Phys. Commun. **185**, 2309 (2014).

[21] V. I. Anisimov, J. Zaanen, and O. K. Andersen, Phys. Rev. B **44**, 943 (1991).

[22] M. Karolak, G. Ulm, T. Wehling, V. Mazurenko, A. Poteryaev, and A. Lichtenstein, J. Electron Spectrosc. Relat. Phenom. **181**, 11 (2010).

[23] A. Hariki, T. Uozumi, and J. Kuneš, Phys. Rev. B **96**, 045111 (2017).

[24] K. Higashi, M. Winder, J. Kuneš, and A. Hariki, Phys. Rev. X **11**, 041009 (2021).

[25] A. Hariki, K. Higashi, T. Yamaguchi, J. Li, C. Kalha, M. Mascheck, S. K. Eriksson, T. Wiell, F. M. F. de Groot, and A. Regoutz, Phys. Rev. B **106**, 205138 (2022).

[26] See Supplemental Material at http://link.aps.org/supplemental/10.1103/PhysRevB.109.205131 for the double-counting dependence of the valence-band and Ni $2p$ core-level XPS spectra.

[27] P. Werner, A. Comanac, L. de' Medici, M. Troyer, and A. J. Millis, Phys. Rev. Lett. **97**, 076405 (2006).

[28] L. Boehnke, H. Hafermann, M. Ferrero, F. Lechermann, and O. Parcollet, Phys. Rev. B **84**, 075145 (2011).

[29] H. Hafermann, K. R. Patton, and P. Werner, Phys. Rev. B **85**, 205106 (2012).

[30] X. Wang, E. Gull, L. de' Medici, M. Capone, and A. J. Millis, Phys. Rev. B **80**, 045101 (2009).

[31] M. Jarrell and J. Gubernatis, Phys. Rep. **269**, 133 (1996).

[32] M. Ghiasi, A. Hariki, M. Winder, J. Kuneš, A. Regoutz, T.-L. Lee, Y. Hu, J.-P. Rueff, and F. M. F. de Groot, Phys. Rev. B **100**, 075146 (2019).

[33] M. Winder, A. Hariki, and J. Kuneš, Phys. Rev. B **102**, 085155 (2020).

[34] K. Momma and F. Izumi, J. Appl. Crystall. **44**, 1272 (2011).

[35] M. Taguchi, M. Matsunami, Y. Ishida, R. Eguchi, A. Chainani, Y. Takata, M. Yabashi, K. Tamasaku, Y. Nishino, T. Ishikawa, Y. Senba, H. Ohashi, and S. Shin, Phys. Rev. Lett. **100**, 206401 (2008).

[36] H. Eisaki, S. Uchida, T. Mizokawa, H. Namatame, A. Fujimori, J. van Elp, P. Kuiper, G. A. Sawatzky, S. Hosoya, and H. Katayama-Yoshida, Phys. Rev. B **45**, 12513 (1992).

[37] M. A. van Veenendaal and G. A. Sawatzky, Phys. Rev. Lett. **70**, 2459 (1993).

[38] A. Hariki, Y. Ichinozuka, and T. Uozumi, J. Phys. Soc. Jpn. **82**, 043710 (2013).

[39] H. Wadati, K. Tanaka, A. Fujimori, T. Mizokawa, H. Kumigashira, M. Oshima, S. Ishiwata, M. Azuma, and M. Takano, Phys. Rev. B **76**, 205123 (2007).

[40] T. Nishikubo, Y. Sakai, K. Oka, T. Watanuki, A. Machida, M. Mizumaki, K. Maebayashi, T. Imai, T. Ogata, K. Yokoyama, Y. Okimoto, S. Koshihara, H. Hojo, T. Mizokawa, and M. Azuma, J. Am. Chem. Soc. **141**, 19397 (2019).

[41] X. F. Hao, A. Stroppa, P. Barone, A. Filippetti, C. Franchini, and S. Picozzi, New J. Phys. **16**, 015030 (2014).

[42] M. Trzhaskovskaya and V. Yarzhemsky, At. Data Nucl. Data Tables **119**, 99 (2018).

[43] M. Trzhaskovskaya, V. Nefedov, and V. Yarzhemsky, At. Data Nucl. Data Tables **77**, 97 (2001).

[44] M. Trzhaskovskaya, V. Nefedov, and V. Yarzhemsky, At. Data Nucl. Data Tables **82**, 257 (2002).

[45] I. Leonov, A. S. Belozerov, and S. L. Skornyakov, Phys. Rev. B **100**, 161112(R) (2019).

[46] G. A. Sawatzky and J. W. Allen, Phys. Rev. Lett. **53**, 2339 (1984).

[47] A. Fujimori, F. Minami, and S. Sugano, Phys. Rev. B **29**, 5225 (1984).

[48] J. Kuneš, V. I. Anisimov, A. V. Lukoyanov, and D. Vollhardt, Phys. Rev. B **75**, 165115 (2007).